

# Effect of isospin asymmetry in nuclear system

Shailesh K. Singh, S. K. Biswal, M. Bhuyan, and S. K. Patra  
*Institute of Physics, Sachivalaya Marg, Bhubaneswar - 751005, India.*

The effect of  $\delta$ - and  $\omega - \rho$ -meson cross couplings on asymmetry nuclear systems are analyzed in the frame-work of an effective Field theory motivated relativistic mean field formalism. The calculations are done on top of the G2 parameter set, where these contributions are absent. We calculate the root mean square radius, binding energy, single particle energy (for the 1<sup>st</sup> and last occupied orbits), density and spin-orbit interaction potential for some selected nuclei and evaluate the  $L_{sym}$ - and  $E_{sym}$ - coefficients for nuclear matter as function of  $\delta$ - and  $\omega - \rho$ -meson coupling strengths. As expected, the influence of these effects are negligible for symmetry nuclear system and these effects are very important for systems with large isospin asymmetry.

PACS numbers: 21.65.Cd, 97.60.Jd, 26.60.Kp, 21.10.Dr, 21.65.-f, 21.65.Mn, 21.10.Ft

## I. INTRODUCTION

In recent years the effective field theory approach to quantum hadrodynamics (QHD) has been studied extensively. The parameter set G2 [1, 2], obtained from the effective field theory motivated Lagrangian (E-RMF) approach, is very successful in reproducing the nuclear matter properties including the structure of neutron star as well as of finite nuclei [3]. This model well reproduce the experimental values of binding energy, root mean square (rms) radii and other finite nuclear properties [4–6]. Similarly, the prediction of nuclear matter properties including the phase transition as well as the properties of compact star are remarkably good [7, 8]. The G2 force parameter is the largest force set available, in the relativistic mean field model. It contains almost all interaction terms of nucleon with mesons, self and cross coupling of mesons upto 4<sup>th</sup> order.

In the effective field theory motivated relativistic mean field (E-RMF) model of Furnstahl et al [1, 2], the coupling of  $\delta$ -meson is not taken into account. Also, the effect of  $\rho$  and  $\omega$  meson cross coupling was neglected. It is soon realized that the importance of  $\delta$  meson [9] and the cross coupling of  $\omega$  and  $\rho$ -mesons [10] can not be neglected while studying the nuclear and neutron matter properties. Horowitz and Piekarewicz [11] studied explicitly the importance of  $\rho$  and  $\omega$  cross coupling to finite nuclei as well as to the properties of neutron star structures. This coupling also influences the nuclear matter properties, like symmetry energy  $E_{sym}$ , slope parameters  $L_{sym}$  and curvature  $K_{sym}$  of  $E_{sym}$  [12]. It is shown in Ref. [3] that the self- and cross couplings of  $\omega$  meson plays an important role to make the nuclear equation of state (EOS) softer.

The observation of Brown [13] and later on by Horowitz and Piekarewicz [11] make it clear that the neutron radius of heavy nuclei have a direct correlation with the equation of state (EOS) of compact star matter. It is shown that the collection of neutron to proton radius difference  $\Delta r = r_n - r_p$  using relativistic and nonrelativistic formalisms show two different patterns. Unfortunately, the error bar in neutron radius makes no difference between

these two pattern. Therefore, the experimental result of JLAB [14] is much awaited. To have a better argument for all this, Horowitz and Piekarewicz [11] introduced  $\Lambda_s$  and  $\Lambda_v$  couplings to take care of the skin thickness in  $^{208}\text{Pb}$  as well as the crust of neutron star. The symmetry energy, and hence the neutron radius, plays an important role in the construction of asymmetric nuclear EOS. Although, the new couplings  $\Lambda_s$  and  $\Lambda_v$  take care of the neutron radius problem, the effective mass splitting between neutron and proton is not taken care. This effect can not be neglected in a highly neutron-rich dense matter system and drip-line nuclei. In addition to this mass splitting, the rms charge radius anomaly of  $^{40}\text{Ca}$  and  $^{48}\text{Ca}$  may be resolved by this scalar-isovector  $\delta$ -meson inclusion to the E-RMF model. Our aim in this paper is to see the effect of  $\delta$ - and  $\rho - \omega$ -mesons couplings in a highly asymmetric system, like asymmetric finite nuclei, neutron star and asymmetric EOS.

The paper is organized as follows: First of all we extended the E-RMF Lagrangian by including the  $\delta$ -meson and the  $\omega - \rho$  cross couplings. The field equations are derived from the extended Lagrangian for finite nuclei. Then the equation of state for nuclear matter and neutron star matters are derived. The calculated results are discussed in section III. In this section, we study the effect of  $\delta$ -meson on asymmetric nuclear matter, including the neutron star. Then, we adopt the calculations for finite nuclei and see the changes in binding energy, radius etc. In the last section, the conclusions are drawn.

## II. FORMALISM

The relativistic treatment of the quantum hadrodynamics (QHD) models automatically include the spin-orbit force, the finite range and the density dependence of the nuclear interaction. The non-linearity of the  $\sigma$ -meson coupling included the 3-body interaction [15], which is currently noticed as an important ingredient for nuclear saturation. The relativistic mean field (RMF) or the E-RMF model has the advantage that, with the proper relativistic kinematics and with the meson properties already known or fixed from the properties of a

small number of finite nuclei, it gives excellent results for binding energies, root-mean-square radii, quadrupole and hexadecapole deformations and other properties of spherical and deformed nuclei [16–20]. The quality of the results is comparable to that found in non-relativistic nuclear structure calculations with effective Skyrme [21] or Gogny [22] forces.

The theory and the equations for finite nuclei and nuclear matter can be found in Refs. [1, 2, 23, 24] and we shall only outline the formalism here. We start from Ref. [1] where the field equations were derived from an energy density functional containing Dirac baryons and classical scalar and vector mesons. Although this energy functional can be obtained from the effective Lagrangian in the Hartree approximation [2, 24], it can also be considered as an expansion in terms of ratios of the meson fields and their gradients to the nucleon mass. The energy density functional for finite nuclei can be written as [2, 23, 24]:

$$\begin{aligned}
\mathcal{E}(r) = & \sum_{\alpha} \varphi_{\alpha}^{\dagger}(r) \left\{ -i\boldsymbol{\alpha} \cdot \boldsymbol{\nabla} + \beta[M - \Phi(r) - \tau_3 D(r)] \right. \\
& + W(r) + \frac{1}{2}\tau_3 R(r) + \frac{1+\tau_3}{2}A(r) \\
& \left. - \frac{i\beta\boldsymbol{\alpha}}{2M} \cdot \left( f_v \boldsymbol{\nabla} W(r) + \frac{1}{2}f_{\rho}\tau_3 \boldsymbol{\nabla} R(r) \right) \right\} \varphi_{\alpha}(r) \\
& + \left( \frac{1}{2} + \frac{\kappa_3}{3!} \frac{\Phi(r)}{M} + \frac{\kappa_4}{4!} \frac{\Phi^2(r)}{M^2} \right) \frac{m_s^2}{g_s^2} \Phi^2(r) \\
& + \frac{1}{2g_s^2} \left( 1 + \alpha_1 \frac{\Phi(r)}{M} \right) (\boldsymbol{\nabla}\Phi(r))^2 - \frac{\zeta_0}{4!} \frac{1}{g_v^2} W^4(r) \\
& - \frac{1}{2g_v^2} \left( 1 + \alpha_2 \frac{\Phi(r)}{M} \right) (\boldsymbol{\nabla}W(r))^2 - \frac{1}{2e^2} (\boldsymbol{\nabla}A(r))^2 \\
& - \frac{1}{2} \left( 1 + \eta_1 \frac{\Phi(r)}{M} + \frac{\eta_2}{2} \frac{\Phi^2(r)}{M^2} \right) \frac{m_v^2}{g_v^2} W^2(r) \\
& - \frac{1}{2g_{\rho}^2} (\boldsymbol{\nabla}R(r))^2 - \frac{1}{2} \left( 1 + \eta_{\rho} \frac{\Phi(r)}{M} \right) \frac{m_{\rho}^2}{g_{\rho}^2} R^2(r) \\
& + \frac{1}{2g_{\delta}^2} (\boldsymbol{\nabla}D(r))^2 - \frac{1}{2} \frac{m_{\delta}^2}{g_{\delta}^2} (D^2(r)) \\
& - \Lambda_v (R^2(r) \times W^2(r)), \tag{1}
\end{aligned}$$

where  $\Phi$ ,  $W$ ,  $R$ ,  $D$  and  $A$  are the fields for  $\sigma, \omega, \rho, \delta$  and photon and  $g_{\sigma}, g_{\omega}, g_{\rho}, g_{\delta}$  and  $\frac{e^2}{4\pi}$  are their coupling constant, respectively. The masses of the mesons are  $m_{\sigma}, m_{\omega}, m_{\rho}$  and  $m_{\delta}$  for  $\Phi_0, V_0, b_0$  and  $\delta_0$ , respectively. In the energy functional, the non-linearity as well as the cross-coupling upto a maximum of 4<sup>th</sup> order is taken into account. This is restricted due the condition  $1 > \frac{f_{field}}{M}$  ( $M$  = nucleon mass) and non-significant contribution of the higher order [4]. The higher non-linear coupling for  $\rho$ - and  $\delta$ -meson fields are not taken in the energy functional, because the expectation values of the  $\rho$ - and  $\delta$ -

fields are order of magnitude less than that of  $\omega$ -field and they have only marginal contribution to finite nuclei. For example, in calculations of the high-density equation of state, Müller and Serot [23] found the effects of a quartic  $\rho$  meson coupling ( $R^4$ ) to be appreciable only in stars made of pure neutron matter. A surface contribution  $-\alpha_3 \Phi (\boldsymbol{\nabla}R)^2 / (2g_{\rho}^2 M)$  was tested in Ref. [25] and it was found to have absolutely negligible effects. We should note, nevertheless, that very recently it has been shown that couplings of the type  $\Phi^2 R^2$  and  $W^2 R^2$  are useful to modify the neutron radius in heavy nuclei while making very small changes to the proton radius and the binding energy [11].

The Dirac equation corresponding to the energy density eqn. (1) becomes

$$\begin{aligned}
\left\{ \begin{aligned} & -i\boldsymbol{\alpha} \cdot \boldsymbol{\nabla} + \beta[M - \Phi(r) - \tau_3 D(r)] + W(r) + \frac{1}{2}\tau_3 R(r) \\ & + \frac{1+\tau_3}{2}A(r) - \frac{i\beta\boldsymbol{\alpha}}{2M} \cdot \left[ f_v \boldsymbol{\nabla} W(r) + \frac{1}{2}f_{\rho}\tau_3 \boldsymbol{\nabla} R(r) \right] \end{aligned} \right\} \varphi_{\alpha}(r) \\
= \varepsilon_{\alpha} \varphi_{\alpha}(r). \tag{2}
\end{aligned}$$

The mean field equations for  $\Phi$ ,  $W$ ,  $R$ ,  $D$  and  $A$  are given by

$$\begin{aligned}
-\Delta\Phi(r) + m_s^2\Phi(r) = & g_s^2 \rho_s(r) - \frac{m_s^2}{M} \Phi^2(r) \left( \frac{\kappa_3}{2} + \frac{\kappa_4}{3!} \frac{\Phi(r)}{M} \right) \\
& + \frac{g_s^2}{2M} \left( \eta_1 + \eta_2 \frac{\Phi(r)}{M} \right) \frac{m_v^2}{g_v^2} W^2(r) \\
& + \frac{\eta_{\rho}}{2M} \frac{g_s^2}{g_{\rho}^2} m_{\rho}^2 R^2(r) + \frac{\alpha_2}{2M} \frac{g_s^2}{g_v^2} (\boldsymbol{\nabla}W(r))^2 \\
& + \frac{\alpha_1}{2M} [(\boldsymbol{\nabla}\Phi(r))^2 + 2\Phi(r)\Delta\Phi(r)] \tag{3}
\end{aligned}$$

$$\begin{aligned}
-\Delta W(r) + m_v^2 W(r) = & g_v^2 \left( \rho(r) + \frac{f_v}{2} \rho_{T}(r) \right) - \frac{1}{3!} \zeta_0 W^3(r) \\
& - \left( \eta_1 + \frac{\eta_2}{2} \frac{\Phi(r)}{M} \right) \frac{\Phi(r)}{M} m_v^2 W(r) \\
& + \frac{\alpha_2}{M} [\boldsymbol{\nabla}\Phi(r) \cdot \boldsymbol{\nabla}W(r) + \Phi(r)\Delta W(r)] \\
& - 2\Lambda_v g_v^2 R^2(r) W(r), \tag{4}
\end{aligned}$$

$$\begin{aligned}
-\Delta R(r) + m_{\rho}^2 R(r) = & \frac{1}{2} g_{\rho}^2 \left( \rho_3(r) + \frac{1}{2} f_{\rho} \rho_{T,3}(r) \right) \\
& - \eta_{\rho} \frac{\Phi(r)}{M} m_{\rho}^2 R(r) - 2\Lambda_v g_{\rho}^2 R(r) W^2(r) \tag{5}
\end{aligned}$$

$$-\Delta A(r) = e^2 \rho_p(r), \tag{6}$$

$$-\Delta D(r) + m_{\delta}^2 D(r) = g_{\delta}^2 \rho_{s3}, \tag{7}$$

where the baryon, scalar, isovector, proton and tensor

densities are

$$\rho(r) = \sum_{\alpha} \varphi_{\alpha}^{\dagger}(r) \varphi_{\alpha}(r), \quad (8)$$

$$\rho_s(r) = \sum_{\alpha} \varphi_{\alpha}^{\dagger}(r) \beta \varphi_{\alpha}(r), \quad (9)$$

$$\rho_3(r) = \sum_{\alpha} \varphi_{\alpha}^{\dagger}(r) \tau_3 \varphi_{\alpha}(r), \quad (10)$$

$$\rho_p(r) = \sum_{\alpha} \varphi_{\alpha}^{\dagger}(r) \left( \frac{1 + \tau_3}{2} \right) \varphi_{\alpha}(r), \quad (11)$$

$$\rho_T(r) = \sum_{\alpha} \frac{i}{M} \nabla \cdot [\varphi_{\alpha}^{\dagger}(r) \beta \alpha \varphi_{\alpha}(r)], \quad (12)$$

$$\rho_{T,3}(r) = \sum_{\alpha} \frac{i}{M} \nabla \cdot [\varphi_{\alpha}^{\dagger}(r) \beta \alpha \tau_3 \varphi_{\alpha}(r)], \quad (13)$$

$$\rho_{s3}(r) = \sum_{\alpha} \varphi_{\alpha}^{\dagger}(r) \tau_3 \beta \varphi_{\alpha}(r), \quad (14)$$

where  $\rho_{s3} = \rho_{sp} - \rho_{sn}$ ,  $\rho_{sp}$  and  $\rho_{sn}$  are scalar densities for proton and neutron respectively. The scalar density  $\rho_s$  is expressed as the sum of proton(p) and neutron(n) densities  $\rho_s = \langle \psi \psi \rangle = \rho_{sp} + \rho_{sn}$ , which are given by

$$\rho_{si} = \frac{2}{(2\pi)^3} \int_0^{k_i} d^3 k \frac{M_i^*}{(k^2 + M_i^{*2})^{\frac{1}{2}}}, \quad i = p, n \quad (15)$$

$k_i$  is the nucleon's Fermi momentum and  $M_p^*$ ,  $M_n^*$  are the proton and neutron effective masses, respectively and can be written as

$$M_p^* = M - g_s \phi_0 - g_{\delta} \delta, \quad (16)$$

$$M_n^* = M - g_s \phi_0 + g_{\delta} \delta. \quad (17)$$

Thus, the  $\delta$  field splits the nucleon effective masses. The baryon density is given by

$$\rho_B = \langle \psi \gamma^0 \psi \rangle = \gamma \int_0^{k_F} \frac{d^3 k}{(2\pi)^3}, \quad (18)$$

where  $\gamma$  is spin or isospin multiplicity ( $\gamma = 4$  for symmetric nuclear matter and  $\gamma = 2$  for pure neutron matter). The proton and neutron Fermi momentum will also split, while they have to fulfill the following condition:

$$\begin{aligned} \rho_B &= \rho_p + \rho_n \\ &= \frac{2}{(2\pi)^3} \int_0^{k_p} d^3 k + \frac{2}{(2\pi)^3} \int_0^{k_n} d^3 k. \end{aligned} \quad (19)$$

Because of the uniformity of the nuclear system for infinite nuclear matter all of the gradients of the fields in Eqs. (1)–(7) vanishes and only the  $\kappa_3$ ,  $\kappa_4$ ,  $\eta_1$ ,  $\eta_2$  and  $\zeta_0$

non-linear couplings remain. Due to the fact that the solution of symmetric nuclear matter in mean field depends on the ratios  $g_s^2/m_s^2$  and  $g_v^2/m_v^2$  [26], we have seven unknown parameters. By imposing the values of the saturation density, total energy, incompressibility modulus and effective mass, we still have three free parameters (the value of  $g_{\rho}^2/m_{\rho}^2$  is fixed from the bulk symmetry energy coefficient  $J$ ). The energy density and pressure of nuclear matter is given by

$$\begin{aligned} \epsilon &= \frac{2}{(2\pi)^3} \int d^3 k E_i^*(k) + \rho(r) W(r) + \frac{1}{2} \rho_3(r) R(r) \\ &\quad + \frac{m_s^2 \Phi^2}{g_s^2} \left( \frac{1}{2} + \frac{\kappa_3}{3!} \frac{\Phi(r)}{M} + \frac{\kappa_4}{4!} \frac{\Phi^2(r)}{M^2} \right) - \frac{1}{4!} \frac{\zeta_0 W^4(r)}{g_v^2} \\ &\quad - \frac{1}{2} m_v^2 \frac{W^2(r)}{g_v^2} \left( 1 + \eta_1 \frac{\Phi}{M} + \frac{\eta_2}{2} \frac{\Phi^2}{M^2} \right) + \frac{1}{2} \frac{m_{\delta}^2}{g_{\delta}^2} (D^2(r)) \\ &\quad - \frac{1}{2} \left( 1 + \frac{\eta_{\rho} \Phi(r)}{M} \right) \frac{m_{\rho}^2}{g_{\rho}^2} R^2(r) - \Lambda_v R^2(r) \times W^2(r), \quad (20) \\ P &= \frac{2}{3(2\pi)^3} \int d^3 k \frac{k^2}{E_i^*(k)} - \frac{m_s^2 \Phi^2}{g_s^2} \left( \frac{1}{2} + \frac{\kappa_3}{3!} \frac{\Phi(r)}{M} + \frac{\kappa_4}{4!} \frac{\Phi^2(r)}{M^2} \right) \\ &\quad + \frac{1}{2} m_v^2 \frac{W^2(r)}{g_v^2} \left( 1 + \eta_1 \frac{\Phi}{M} + \frac{\eta_2}{2} \frac{\Phi^2}{M^2} \right) + \frac{1}{4!} \frac{\zeta_0 W^4(r)}{g_v^2} \\ &\quad + \frac{1}{2} \left( 1 + \frac{\eta_{\rho} \Phi(r)}{M} \right) \frac{m_{\rho}^2}{g_{\rho}^2} R^2(r) + \Lambda_v R^2(r) \times W^2(r) \\ &\quad - \frac{1}{2} \frac{m_{\delta}^2}{g_{\delta}^2} (D^2(r)), \quad (21) \end{aligned}$$

where  $E_i^*(k) = \sqrt{k^2 + M_i^{*2}}$  ( $i = p, n$ ). In the context of density functional theory, it is possible to parametrize the exchange and correlation effects through local potentials (Kohn–Sham potentials), as long as those contributions be small enough [27]. The Hartree values are the ones that control the dynamics in the relativistic Dirac–Bröcker–Hartree–Fock (DBHF) calculations. Therefore, the local meson fields in the RMF formalism can be interpreted as Kohn–Sham potentials and in this sense equations (3)–(7) include effects beyond the Hartree approach through the non-linear couplings [1, 2, 24].

### III. RESULTS AND DISCUSSIONS

Our calculated results are shown in Figs. (1 – 10) and Table I for both finite nuclei and infinite nuclear systems. The effect of  $\delta$ -meson and the crossed coupling constant  $\Lambda_v$  of  $\omega - \rho$  fields on some selected nuclei like  $^{48}\text{Ca}$  and  $^{208}\text{Pb}$  are demonstrated in Figs. 1 – 4 and the nuclear matter outcomes are displayed in rest of the figures and table. In one of our recent publication [12], the explicit dependence of  $\Lambda_v(\omega - \rho)$  on nuclear matter properties are shown and it is found that it has significant implication on various physical properties, like mass and radius of neutron star and  $E_{\text{sym}}$  asymmetry energy and its slope parameter  $L_{\text{sym}}$  for infinite nuclear matter system at high densities. Here, only the influence of  $\Lambda_v$  on finite nuclei and that of  $g_\delta$  on both finite and infinite nuclear systems are studied.

#### A. Finite Nuclei

In this section we analyzed the effects of  $\delta$  meson and  $\Lambda_v$  coupling in finite nuclei. For this, we calculate the binding energy (BE), rms radii ( $r_n$ ,  $r_p$ ,  $r_{ch}$ ,  $r_{rms}$ ), and energy of first and last filled orbitals of  $^{48}\text{Ca}$  and  $^{208}\text{Pb}$  with  $g_\delta$  and  $\Lambda_v$ . The finite size of the nucleon is taken into account for the charge radius using the relation  $r_{ch} = \sqrt{r_p^2 + 0.64}$ . The results are shown in Figs. 1, 2.

In our calculations, while analyzing the effect of  $g_\delta$ , we keep  $\Lambda_v = 0$  and vice versa. From the figures, it is evident that the binding energy, radii and single particle levels  $\epsilon_{n,p}$  affected drastically with  $g_\delta$  contrary to the effect of  $\Lambda_v$ . A careful inspection shows a slight decrease of  $r_n$  with the increase of  $\Lambda_v$  consistent with the analysis of [28]. Again, it is found that the binding energy increases with increasing of the coupling strength upto  $g_\delta \sim 1.5$  and no convergence solution available beyond this value. Similar to the  $g_\delta$  limit, there is limit for  $\Lambda_v$  also, beyond which no solution exist. From the anatomy of  $g_\delta$  on  $r_n$  and  $r_p$ , we find their opposite trend in size. That means the value of  $r_n$  decreases and  $r_p$  increases with  $g_\delta$  for both  $^{48}\text{Ca}$  and  $^{208}\text{Pb}$ . It so happens that both the radii meet at a point near  $g_\delta = 1.0$  (Fig 1 and Fig. 2) and again shows reverse character on increasing  $g_\delta$ , i.e., the neutron skin thickness ( $r_n - r_p$ ) changes its sign with  $g_\delta$ . This interesting results may help us to settle the charge radius anomaly of  $^{40}\text{Ca}$  and  $^{48}\text{Ca}$ .

In Fig. 1(c), we have shown the first ( $1s^{n,p}$ ) and last ( $1f^n$  and  $2s^p$ ) filled orbitals for  $^{48}\text{Ca}$  as a function of  $g_\delta$  and  $\Lambda_v$ . The effect of  $\Lambda_v$  is marginal, i.e., almost negligible on  $\epsilon_{n,p}$  orbitals. However, this is significance with the increasing value of  $g_\delta$ . The top most filled orbital even crosses each other at  $g_\delta \sim 1$ , although initially, it is well separated. On the other hand, the first filled orbital  $1s$  both for proton and neutron get separated more and more with  $g_\delta$ , which has almost same single particle energy  $\epsilon_{n,p}$  at  $g_\delta = 0$ . We get similar trend for  $^{208}\text{Pb}$ , which

FIG. 1: Binding energy (BE), root mean square radius and first ( $1s^{n,p}$ ) and last ( $1f^n$ ,  $2s^p$ ) occupied orbitals for  $^{48}\text{Ca}$  as a function of  $g_\delta$  and  $\Lambda_v$ .

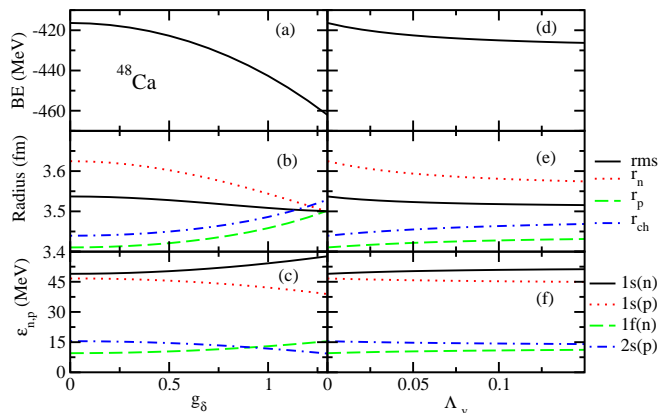
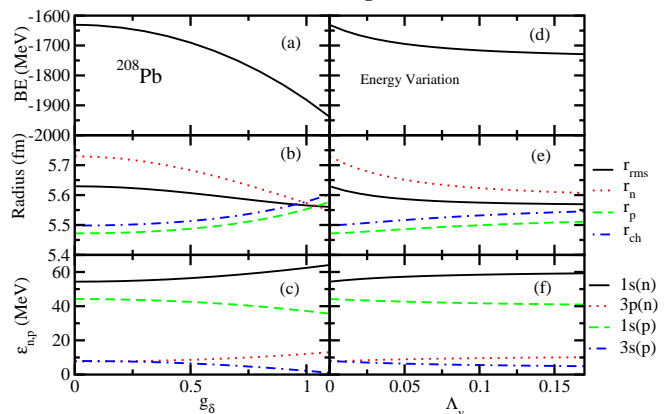


FIG. 2: Same as Fig. 1 for  $^{208}\text{Pb}$ .



is shown in Fig. 2(c). In both the representative cases, we notice orbital flipping only for the last filled levels.

The nucleon density distribution (proton  $\rho_p$  and neutron  $\rho_n$ ) and spin orbit interaction potential  $U_{so}$  of finite nuclei are shown in Figs. 3 and 4. The calculations are done with two different values of  $g_\delta$  and  $\Lambda_v$  as shown in the figures. Here, the solid line is drawn for initial and dotted one is for the limiting values. In Fig. 3(a), we have depicted the neutron, proton and total density distribution for  $^{48}\text{Ca}$  at values of  $g_\delta = 0.0$  and  $1.3$ . Comparing Figs. 3(a) and 3(c), one can see that the sensitivity of  $g_\delta$  is more than  $\Lambda_v$  on density distribution. The spin-orbit potential  $U_{so}$  of  $^{48}\text{Ca}$  with different values of  $g_\delta$  are shown in Fig. 3(b) and for  $\Lambda_v$  in Fig. 3(d). Similarly, we have given these observables for  $^{208}\text{Pb}$  in Fig. 4. In general, for light mass region both coupling constants  $g_\delta$  and  $\Lambda_v$  are less effective in density distribution and spin-orbit potential. It is clear from this analysis that the coupling strength of  $\delta$ -meson is more influential than the isoscalar-vector and isovector-vector cross coupling. This effect is mostly confined to the central region of the nucleus.

FIG. 3: The neutron, proton and total density with radial coordinate  $r(fm)$  at different values of  $g_\delta$  (a) and  $\Lambda_v$  (c). The variation of spin-orbit potential for proton and neutron are shown in (b) and (d) by keeping the same  $g_\delta$  and  $\Lambda_v$  as (a) and (c) respectively.

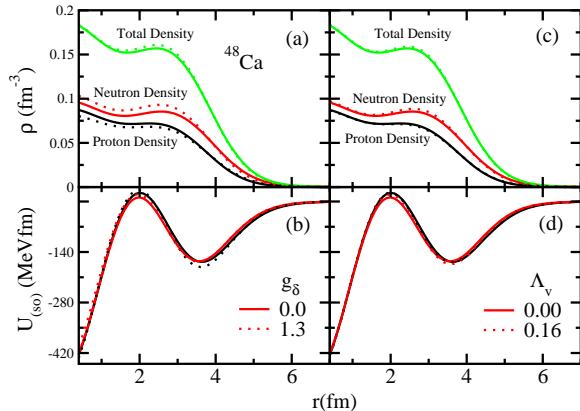
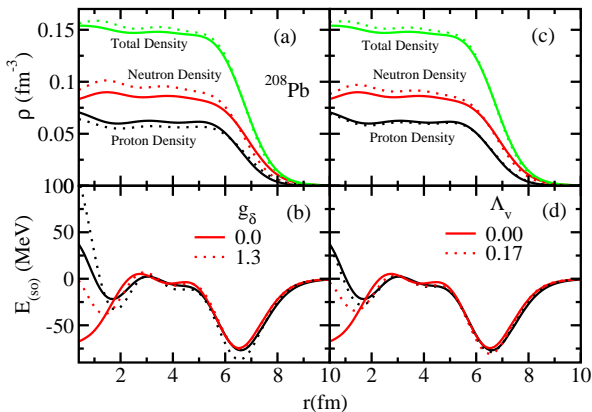


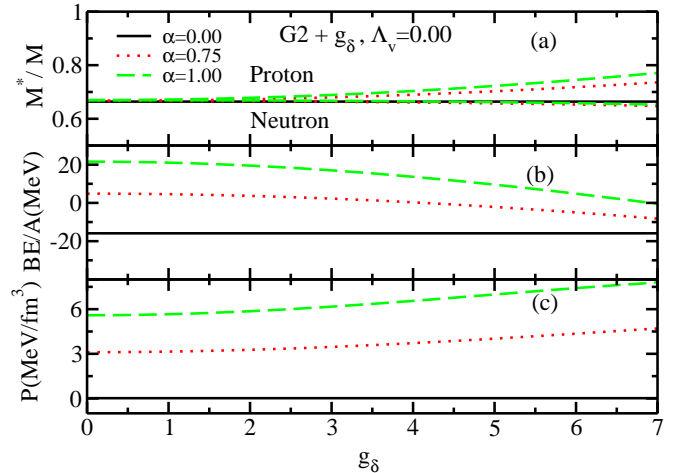
FIG. 4: Same as Fig. 3 for  $^{208}\text{Pb}$ .



## B. Nuclear Matter

In this section, we do calculation for nuclear matter properties like energy and pressure densities, symmetry energy, radii and mass of the neutron star using  $\omega - \rho$  and  $\delta$  couplings on top of G2 parametrization. Recently, it is reported [12] that the  $\omega - \rho$  cross coupling plays a vital role for nuclear matter system on important physical observables like equation of state, symmetry energy coefficient,  $L_{sym}$  coefficient etc. A detail account is available in Ref. [12] for  $\omega - \rho$  coupling on nuclear matter system. The main aim of this section is to take  $\delta$  meson as an additional degree of freedom in our calculations and elaborate the effect on nuclear matter system within G2 parameter set. In highly asymmetric system like neutron star and

FIG. 5: Variation of nucleonic effective masses, binding energy per particle (BE/A) and pressure density as a function of  $g_\delta$  on top of G2 parameter set for nuclear matter.



supernova explosion, the contribution of  $\delta$  meson is important. This is because of the high asymmetry due to the isospin as well as the difference in neutron and proton masses. Here, in the calculations the  $\beta$ -equilibrium and charge neutrality conditions are not considered. We only varies the neutron and proton components with an asymmetry parameter  $\alpha$ , defined as  $\alpha = \frac{\rho_n - \rho_p}{\rho_n + \rho_p}$ . The splitting in nucleon masses is evident from equations (16) and (17) due to the inclusion of isovector scalar  $\delta$ -meson. For  $\alpha=0.0$ , the nuclear matter system is purely symmetrical and for other non-zero value of  $\alpha$ , the system get more and more asymmetry. For  $\alpha = 1.0$ , it is a case of pure neutron matter.

In Fig. 5(a), the effective masses of proton and neutron are given as a function of  $g_\delta$ . As we have mentioned,  $\delta$ -meson is responsible for the splitting of effective masses (Eqns. (16) and (17)), this splitting increases continuously with coupling strength  $g_\delta$ . In Fig. 5, the splitting is shown for few representative cases at  $\alpha=0.0$ , 0.75 and 1.0. The solid line is for  $\alpha=0.0$  and  $\alpha=0.75$ , 1.0 are shown by dotted and dashed line, respectively. From the figure, it is clear that the effective mass is unaffected for symmetric matter. The proton effective mass  $M_p^*$  is above the reference line with  $\alpha = 0$  and the neutron effective mass always lies below it. The effect of  $g_\delta$  on binding energy per nucleon is shown in Fig. 5(b) and pressure density in Fig. 5(c). One can easily see the effect of  $\delta$  meson interaction on the energy and pressure density of the nuclear system. The energy and pressure density show opposite trend to each other with the increase function of  $g_\delta$ .

### C. Energy and Pressure Density

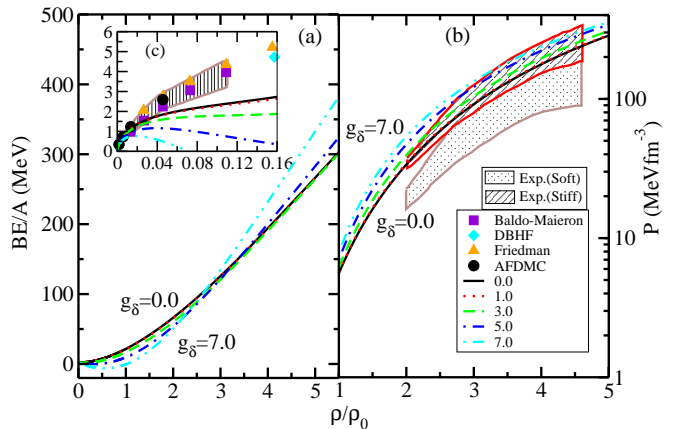
We analyze the binding energy per nucleon and pressure density including the contribution of  $\delta$ -meson in the G2 Lagrangian as a function of density. As it is mentioned earlier, the addition of  $\delta$ -meson is done due to its importance on asymmetry nuclear matter as well as to make a full fledged E-RMF model. This is tested by calculating the observables at different values of  $\delta$ -meson coupling strength  $g_\delta$ . In Fig. 6, the calculated  $BE/A$  and  $\mathcal{P}$  for pure neutron matter with baryonic density for different  $g_\delta$  are shown. Unlike to the small value of  $g_\delta$  upto 1.5 in finite nuclei, the instability arises at  $g_\delta=7.0$  in nuclear matter. Of course, this limiting value of  $g_\delta$  depends on the asymmetry of the system.

In Fig. 6(a), we have given  $BE/A$  for different values of  $g_\delta$ . It is seen from Fig. 6(a), the binding increases with  $g_\delta$  in the lower density region and maximum value of binding energy is  $\sim 7$  MeV for  $g_\delta=7.0$ . On the other hand, in higher density region, the binding energy curve for finite  $g_\delta$  crosses the one with  $g_\delta=0.0$ . That means, the EOS with  $\delta$ -meson is stiffer than the one with pure G2 parametrization. As a result, one get a heavier mass of the neutrons star, which suited with the present experimental finding [29]. For comparing the data at lower density (dilute system,  $0 < \rho/\rho_0 < 0.16$ ) the zoomed version of the region is shown as an inset Fig. 6(c) inside Fig. 6(a). From the zoomed inset portion, it is clearly seen that the curves with various  $g_\delta$  at  $\alpha = 1.0$  (pure neutron matter) deviate from other theoretical predictions, such as Baldo-Maieron [30], DBHF [31], Friedman [32], auxiliary-field diffusion Monte Carlo (AFDMC) [33] and Skyrme interaction [34]. This is an inherited problem in the RMF or E-RMF formalisms, which need more theoretical attention. Similarly, the pressure density for different values of  $g_\delta$  with G2 parameter set are given in Fig. 6(b). At high density we can easily see that the curve becomes more stiffer with the coupling strength  $g_\delta$ . The experimental constraint of equation of state obtained from heavy ion flow data for both stiff and soft EOS is also displayed for comparison in the region  $2 < \rho/\rho_0 < 4.6$  [35]. Our results match with the stiff EOS data of Ref. [35].

### D. Symmetry Energy

The symmetric energy  $E_{sym}$  is important in infinite nuclear matter and finite nuclei, because of isospin dependence in the interaction. The isospin asymmetry arises due to the difference in densities and masses of the neutron and proton, respectively. The density type isospin asymmetry is taken care by  $\rho$  meson (isovector-vector meson) and mass asymmetry by  $\delta$ -meson (isovector-scalar meson). The expression of symmetry energy  $E_{sym}$  is a combine expression of  $\rho$ - and  $\delta$ -mesons, which is defined as [4, 9, 36, 37]:

FIG. 6: Energy per particle and pressure density with respect to density with various  $g_\delta$ .



$$E_{sym}(\rho) = E_{sym}^{kin}(\rho) + E_{sym}^{\rho}(\rho) + E_{sym}^{\delta}(\rho), \quad (22)$$

with

$$E_{sym}^{kin}(\rho) = \frac{k_F^2}{6E_F^*}; \quad E_{sym}^{\rho}(\rho) = \frac{g_\rho^2 \rho}{8m_\rho^{*2}} \quad (23)$$

and

$$E_{sym}^{\delta}(\rho) = -\frac{1}{2}\rho \frac{g_\delta^2}{m_\delta^2} \left(\frac{m^*}{E_F}\right)^2 u_\delta(\rho, m^*). \quad (24)$$

The last function  $u_\delta$  is from the discreteness of the Fermi momentum. This momentum is quite large in nuclear matter system and can be treated as a continuum and continuous system. The function  $u_\delta$  is defined as:

$$u_\delta(\rho, m^*) = \frac{1}{1 + 3\frac{g_\delta^2}{m_\delta^2}} \left(\frac{\rho^s}{m^*} - \frac{\rho}{E_F}\right). \quad (25)$$

In the limit of continuum, the function  $u_\delta \approx 1$ . The whole symmetry energy ( $E_{sym}^{kin} + E_{sym}^{pot}$ ) arises from  $\rho$ - and  $\delta$ -mesons is given as:

$$E_{sym}(\rho) = \frac{k_F^2}{6E_F^*} + \frac{g_\rho^2 \rho}{8m_\rho^{*2}} - \frac{1}{2}\rho \frac{g_\delta^2}{m_\delta^2} \left(\frac{m^*}{E_F}\right)^2 u_\delta(\rho, m^*) \quad (26)$$

where the effective energy  $E_F^* = \sqrt{(k_F^2 + m^{*2})}$ ,  $k_F$  is the Fermi momentum and the effective mass  $m^* = m - g_s \phi_0 \pm g_\delta \delta_0$ . The effective mass of the  $\rho$ -meson modified, because of cross coupling of  $\rho - \omega$  and is given by

$$m_\rho^{*2} = \left(1 + \eta_\rho \frac{g_\sigma \sigma}{m_B}\right) m_\rho^2 + 2g_\rho^2 (\Lambda_v g_v^2 \omega_0^2). \quad (27)$$

The cross coupling of isoscalar-isovector mesons ( $\Lambda_v$ ) modified the density dependent of  $E_{sym}$  without affecting

the saturation properties of the symmetric nuclear matter (SNM). This is explained explicitly in Ref. [12] and no need special attention here. In E-RMF model with pure G2 set, the symmetric nuclear matter saturates at  $\rho_0 = 0.153 \text{ fm}^{-3}$ ,  $BE/A = 16.07 \text{ MeV}$ , compressibility  $K_0 = 215 \text{ MeV}$  and symmetry energy of  $E_{sym} = 36.42 \text{ MeV}$  [1, 2].

In the numerical calculation, the coefficient of symmetry energy  $E_{sym}$  is obtained by the energy difference of symmetry and pure neutron matter at saturation and it is defined by Eqn. (26) for a quantitative description at various densities. Our results for  $E_{sym}$  are compared in Fig. 7 with experimental heavy ion collision (HIC) data [38] and other theoretical predictions of non-relativistic Skyrme-Hartree-Fock model. The calculation is done for pure neutron matter with different values of  $g_\delta$ , which are compared with two selective force parameter sets GSkII [39] and Skxs20 [40]. For more discussion one can see Ref. [34], where 240 different Skyrme parametrizations are used. Here in our calculation, as usual  $\Lambda_v = 0$  to see the effect of  $\delta$ -meson coupling on  $E_{sym}$ . In this figure, shaded region represent the HIC data [38] within  $0.3 < \rho/\rho_0 < 1.0$  region and the symbols square and circle represent the SHF results for GSkII and Skxs20 respectively. Analysing Fig. 7,  $E_{sym}$  of G2 matches with the shaded region in low density region, however as the density increases, the value of  $E_{sym}$  moves away. Again, the symmetry energy becomes softer by increasing the value of coupling strength  $g_\delta$ . For higher value of  $g_\delta$ , again the curve moves far from the empirical shaded area. In this way, we can fix the limiting constraint on coupling strength of  $\delta$ -meson and nucleon. Similar to the finite nuclear case, the nuclear matter system becomes unstable for excessive value of  $g_\delta (> 7.0)$ . This constrained may help to improve the G2+ $g_\delta$  parameter set for both finite and infinite nuclear systems.

The symmetry energy of a nuclear system is a function of baryonic density  $\rho$ , hence can be expanded in a Taylor series around the saturation density  $\rho_0$  as (26):

$$E_{sym}(\rho) = E_0 + L_{sym}\mathcal{Y} + \frac{1}{2}K_{sym}\mathcal{Y}^2 + O[\mathcal{Y}^3], \quad (28)$$

where  $E_0 = E_{sym}(\rho = \rho_0)$ ,  $\mathcal{Y} = \frac{\rho - \rho_0}{3\rho_0}$  and the coefficients  $L_{sym}$  and  $K_{sym}$  are defined as:

$$L_{sym} = 3\rho \left( \frac{\partial E_{sym}}{\partial \rho} \right)_{\rho=\rho_0}, \quad K_{sym} = 9\rho^2 \left( \frac{\partial^2 E_{sym}}{\partial \rho^2} \right)_{\rho=\rho_0} \quad (29)$$

Here  $L_{sym}$  is the slope parameter defined as the slope of  $E_{sym}$  at saturation. The quantity  $K_{sym}$  represents the curvature of  $E_{sym}$  with respect to density. A large number of investigation have been made to fix the value of  $E_{sym}$ ,  $L_{sym}$  and  $K_{sym}$  [12, 34, 38, 41–44]. In Fig. 9, we have given the symmetry energy with its first derivative at saturation density with different values of coupling strength starting from  $g_\delta = 0.0 - 7.0$ . The variation of  $E_{sym}$ ,  $L_{sym}$  and  $K_{sym}$  with  $g_\delta$  are listed in Table I. The variation in symmetry energy takes place from 45.09 to

FIG. 7: Symmetry energy  $E_{sym}$  (MeV) of neutron matter with respect to different value of  $g_\delta$  on top of G2 parameter set. The heavy ion collision (HIC) experimental data [38] (shaded region) and non-relativistic Skyrme GSkII [39], and Skxs20 [40] predictions are also given.  $\Lambda_v=0.0$  is taken.

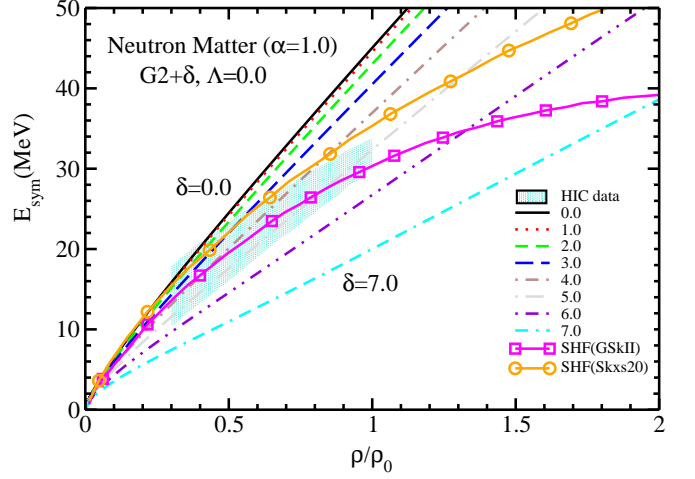
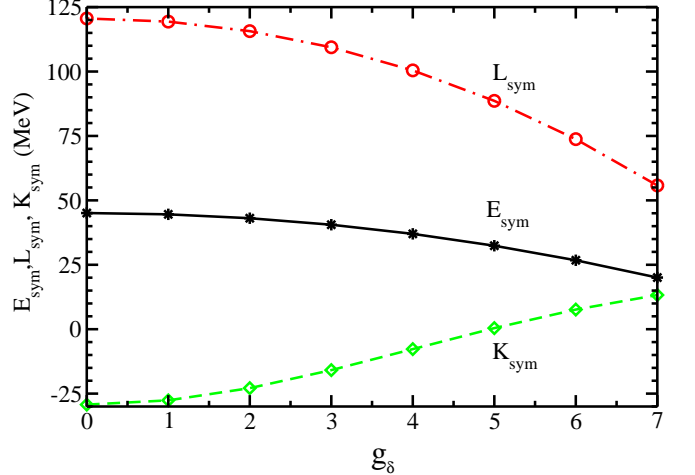


FIG. 8: Symmetry energy  $E_{sym}$  (MeV), slope coefficients  $L_{sym}$  (MeV) and  $K_{sym}$  (MeV) at different  $g_\delta$  with  $\Lambda_v=0.0$ .



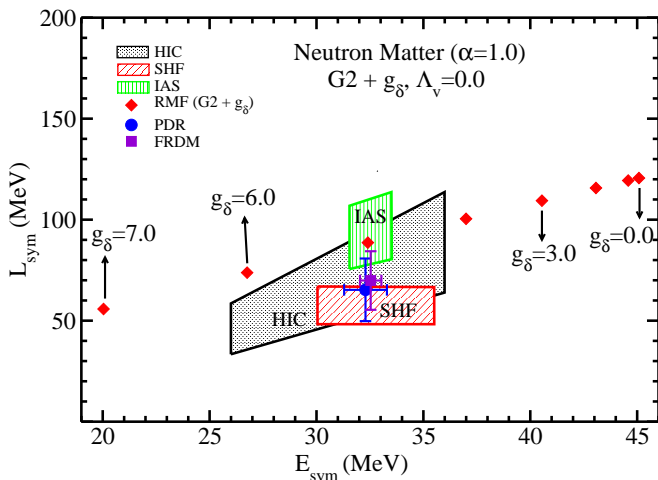
20.04 MeV,  $L_{sym}$  from 120.60 to 55.78 MeV and  $K_{sym}$  from  $-29.28$  to  $13.27 \text{ MeV}$  at saturation density corresponding to  $0.0 < g_\delta < 7.0$ . From this investigation, one can see that G2 set is not sufficient to predict this constrained on  $E_{sym}$  and  $L_{sym}$ . It is suggestive to introduce the  $\delta$ -meson as an extra degree of freedom into the model to bring the data within the prediction of experimental and other theoretical constraints.

The above tabulated results are also depicted in Fig. 8 to get a graphical representation of  $E_{sym}$ ,  $L_{sym}$  and  $K_{sym}$ . The values of  $E_{sym}$  is marginally effective with the  $\delta$ -meson coupling strength. However, in the same time  $L_{sym}$  and  $K_{sym}$  vary substantially as shown in the figure. The slope parameter  $L_{sym}$  decreases almost exponentially opposite to the similar exponential increase of  $K_{sym}$ . At large value of  $g_\delta$  all the three quantities almost

TABLE I: The symmetry energy  $E_{sym}$  (MeV), slope coefficient  $L_{sym}$  (MeV) and  $K_{sym}$  (MeV) at different values of  $g_\delta$ .

$g_\delta$	$E_{sym}$	$L_{sym}$	$K_{sym}$
0.0	45.09	120.60	-29.28
1.0	44.58	119.37	-27.61
2.0	43.07	115.67	-22.87
3.0	40.55	109.41	-15.87
4.0	37.00	100.44	-7.72
5.0	32.40	88.61	0.43
6.0	26.76	73.77	7.61
7.0	20.04	55.78	13.27

FIG. 9: Constraints on  $E_{sym}$  with its first derivative, i.e.,  $L_{sym}$  at saturation density for neutron matter. The experimental results of HIC [38], PDR [45, 46] and IAS [47] are given. The theoretical prediction of finite range droplet model (FRDM) and Skyrme parametrization are also given [48], SHF [34].



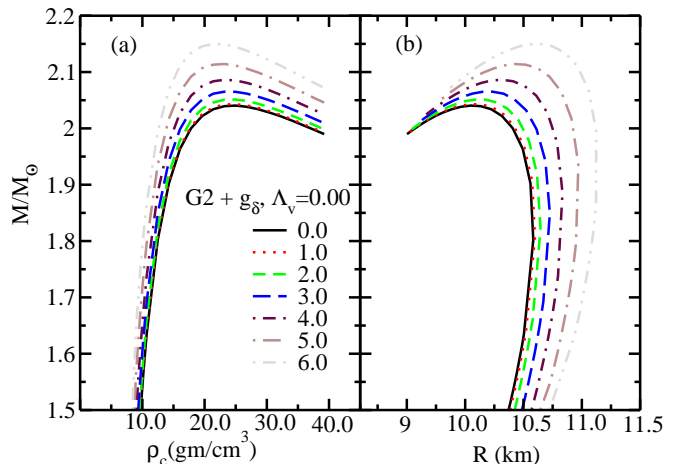
emerge very closely to the similar region.

### E. Neutron Star

In this section, we study the effect of  $\delta$ -meson on mass and radius of neutron star. Recently, experimental observation predicts the constraint on mass of neutron star and its radius [29]. This observation suggests that the theoretical models should predict the star mass and radius as  $M \geq (1.97 \pm 0.04)M_\odot$  and  $11 < R(km) < 15$ . Keeping this point in mind, we calculate the mass and radius of neutron star and analyzed their variation with  $g_\delta$ .

In the interior part of neutron star, the neutron chemical potential exceeds the combined mass of the proton and electron. Therefore, asymmetric matter with an admixture of electrons rather than pure neutron matter, is a more likely composition of matter in neutron star interiors. The concentrations of neutrons, protons and electrons can be determined from the condition of

FIG. 10: The mass and radius of neutron star at different values of  $g_\delta$ . (a)  $M/M_\odot$  with neutron star density ( $\text{gm}/\text{cm}^3$ ), (b)  $M/M_\odot$  with neutron star radius (km).



$\beta$ -equilibrium  $n \leftrightarrow p + e + \bar{\nu}$  and from charge neutrality, assuming that neutrinos are not degenerate. Here  $n$ ,  $p$ ,  $e$ ,  $\nu$  are have usual meaning as neutron, proton, electron and neutrino. In momentum conservation condition  $\nu_n = \nu_p + \nu_e$ ,  $n_p = n_e$ , where  $\nu_n = \mu_n - g_\omega V_0 + \frac{1}{2}g_\rho b_0$  and  $\nu_p = \mu_p - g_\omega V_0 - \frac{1}{2}g_\rho b_0$  with  $\mu_n = \sqrt{(k_{fn}^2 + M_n^{*2})}$  and  $\mu_p = \sqrt{(k_{fp}^2 + M_p^{*2})}$  are the chemical potential, and  $k_{fn}$  and  $k_{fp}$  are the Fermi momentum for neutron and proton, respectively. Imposing this conditions, in the expressions of  $\mathcal{E}$  and  $\mathcal{P}$  (Eqns. 20 - 21), we evaluate  $\mathcal{E}$  and  $\mathcal{P}$  as a function of density. To calculate the star structure, we use the Tolman-Oppenheimer-Volkoff (TOV) equations for the structure of a relativistic spherical and static star composed of a perfect fluid were derived from Einstein's equations [49], where the pressure and energy densities obtained from equations (20) and (21) are the inputs. The TOV equation is given by [49]:

$$\frac{d\mathcal{P}}{dr} = -\frac{G}{r} \frac{[\mathcal{E} + \mathcal{P}][M + 4\pi r^3 \mathcal{P}]}{(r - 2GM)}, \quad (30)$$

$$\frac{dM}{dr} = 4\pi r^2 \mathcal{E}, \quad (31)$$

with  $G$  as the gravitational constant and  $M(r)$  as the enclosed gravitational mass. We have used  $c = 1$ . Given the  $\mathcal{P}$  and  $\mathcal{E}$ , these equations can be integrated from the origin as an initial value problem for a given choice of central energy density, ( $\varepsilon_c$ ). The value of  $r$  ( $= R$ ), where the pressure vanishes defines the surface of the star.

The results of mass and radius with various  $\delta$ -meson coupling strength  $g_\delta$  is shown in Fig. 10. In left panel, the neutron star mass with density ( $\text{gm}/\text{cm}^3$ ) is given, where we can see the effect of the newly introduced extra degree of freedom  $\delta$ -meson into the system. On the

right side of the figure, [Fig. 10],  $M/M_\odot$  is depicted with respect to radius (km), where  $M$  is the mass of the star and  $M_\odot$  is the solar mass. The  $g_\delta$  coupling changes the star mass by  $\sim 5.41\%$  and radius by  $5.39\%$  with a variation of  $g_\delta$  from 0 to 6.0. From this observation, we can say that  $\delta$ -meson is important not only for asymmetry system normal density, but also substantially effective in high density system. If we compare this results with the previous results [12], i.e., with the effects of cross coupling of  $\omega - \rho$  on mass and radius of neutron star, the effects are opposite to each other. That means, the star masses decreases with  $\Lambda_v$ , whereas it is increases with  $g_\delta$ . Thus a finer tuning in mass and radius of neutron star is possible by a suitable adjustment on  $g_\delta$  value in the extended parametrization of  $G2 + \Lambda_v + g_\delta$  to keep the star properties within the recent experimental observations [29].

#### IV. SUMMARY AND CONCLUSIONS

In summary, we rigorously discussed the effects of cross coupling of  $\omega - \rho$ -mesons in finite nuclei on top of the pure G2 parameter set. The variation of binding energy, rms radii and energy levels of protons and neutrons are analyzed with increasing values of  $\Lambda_v$ . The change in neutron distribution radius  $r_n$  with  $\Lambda_v$  is found to be substantial compared to the less effectiveness of binding energy and proton distribution radius for the two repre-

sentative nuclei  $^{48}\text{Ca}$  and  $^{208}\text{Pb}$ . Thus, to fix the neutrons distribution radius depending on the outcome of PREX experimental [14] result, the inclusion of  $\Lambda_v$  coupling strength is crucial. As it is discussed widely by various authors [12], the role of  $\omega - \rho$ -mesons in the nuclear matter system is important on nuclear equation of states.

We emphasized strongly the importance of the effect of the extra degree of freedom, i.e.,  $\delta$ -meson coupling into the standard RMF or E-RMF model, where, generally it is ignored. We have seen the effect of this coupling strength of  $\delta$ -meson with nucleon in finite and neutron matter is substantial and very different in nature, which may be extremely helpful to fix various experimental constraints. For example, with the help of  $g_\delta$ , it is possible to modify the binding energy, charge radius and flipping of the orbits in asymmetry finite nuclei systems. The nuclear equation of state can be made stiffer with the inclusion of  $\delta$ -meson coupling. On the other hand, softening of symmetry energy is also possible with the help of this extra degree of freedom. In compact system, it is possible to fix the limiting values of  $g_\delta$  and  $\Lambda_v$  by testing the effect on available constraints on symmetry energy and its first derivative with respect to the matter density. This coupling may be extremely useful to fix the mass and radius of neutron star keeping in view of the recent observation [29].

- 
- [1] R. J. Furnstahl, B. D. Serot and H. B. Tang, Nucl. Phys. A **598**, 539 (1996).
  - [2] R. J. Furnstahl, B. D. Serot and H. B. Tang, Nucl. Phys. A **615**, 441 (1997).
  - [3] P. Arumugam, B. K. Sharma, P. K. Sahu, S. K. Patra, Tapas Sil, M. Centelles and X. Viñas, Phys. Lett. B **601** 51 (2004).
  - [4] M. Del Estal, M. Centelles, X. Viñas and S. K. Patra, Phys. Rev. C **63**, 044321 (2001).
  - [5] M. Del Estal, M. Centelles, X. Viñas and S. K. Patra, Phys. Rev. C **63**, 024314 (2001).
  - [6] Tapas Sil, S. K. Patra, B. K. Sharma, M. Centelles and X. Viñas, Phys. Rev. C **69**, 044315 (2004).
  - [7] P. Arumugam, B. K. Sharma, P. K. Sahu, S. K. Patra, Tapas Sil, M. Centelles and X. Viñas, Phys. Lett. B **601**, 51 (2004).
  - [8] B. K. Sharma, P. K. Panda and S. K. Patra, Phys. Rev. C **75**, 035808 (2007).
  - [9] S. Kubis and M. Kutschera, Phys. Lett. B **399**, 191 (1997).
  - [10] J. K. Bunta and S. Gmuca, Phys. Rev. C **68**, 054318 (2003).
  - [11] C. J. Horowitz and J. Pickarewicz, Phys. Rev. Lett. **86**, 5647 (2001); Phys. Rev. C **64**, 062802 (R) (2001).
  - [12] S. K. Singh, M. Bhuyan, P. K. Panda and S. K. Patra, J. Phys. G: Nucl. Part. Phys. **40**, 085104 (2013).
  - [13] B. A. Brown, Phys. Rev. Lett. **85**, 5296 (2000).
  - [14] S. Abrahamyan et al. *arXiv.1201.2568v2* (2012).
  - [15] L. I. Schieff, Phys. Rev. **84**, 1 (1951).
  - [16] Y. K. Gambhir, P. Ring and A. Thimet, Ann. Phys. (N.Y.) **198**, 132 (1990).
  - [17] S. K. Patra and C. R. Praharaaj, Phys. Rev. C **44**, 2552 (1991).
  - [18] M. Rufa, P. -G. Reinhard, J. A. Maruhn, W. Greiner and M. R. Strayer, Phys. Rev. C **38**, 390 (1988).
  - [19] P. -G. Reinhard, M. Rufa, J. Maruhn, W. Greiner and J. Friedrich, Z. Phys. A **323**, 13 (1986).
  - [20] M. Sharma, G. A. Lalazissis and P. Ring, Phys. Lett. B **317**, 9 (1993).
  - [21] D. Vautherin and D. M. Brink, Phys. Rev. C **5**, 626 (1972).
  - [22] J. Decharge and D. Gogny, Phys. Rev. C **21**, 1568 (1980).
  - [23] H. Müller and B. D. Serot, Nucl. Phys. A **606**, 508 (1996).
  - [24] B. D. Serot and J. D. Walecka, Int. J. Mod. Phys. E **6**, 515 (1997).
  - [25] M. Del Estal, M. Centelles and X. Viñas, Nucl. Phys. A **650**, 443 (1999).
  - [26] B. D. Serot and J. D. Walecka, Adv. Nucl. Phys. **16**, 1 (1986).
  - [27] W. Kohn and L. J. Sham, Phys. Rev. **140**, A1133 (1965).
  - [28] M. Centelles, S. K. Patra, X. Roca-Maza, B. K. Sharma, P. D. Stevenson, X. Viñas, J. Phys. G **37**, 075107 (2010).
  - [29] P. B. Demorest, T. Pennucci, S. M. Ransom, M. S. E. Roberts and J. W. T. Hessels, Nature **467**, 1081 (2010).
  - [30] M. Baldo and C. Maieron, Phys. Rev. C **77**, 015801 (2008).

- [31] J. Margueron, H. Sagawa and K. Hagino, *Phys. Rev. C* **77**, 054309 (2008).
- [32] B. Friedman and V. R. Pandharipande, *Nucl. Phys. A* **361**, 502 (1981).
- [33] S. Gandol, A. Yu. Illarionov, S. Fantoni, F. Pederiva and K. E. Schmidt, *Phys. Rev. Lett.* **101**, 132501 (2008).
- [34] M. Dutra et al., *Phys. Rev. C* **85**, 035201 (2012).
- [35] P. Danielewicz, R. Lacey and W. G. Lynch, *Science* **298**, 1592 (2002).
- [36] T. Matsui, *Nucl. Phys. A* **370**, 365 (1981).
- [37] X. Roca-Maza, X. Viñas, M. Centelles, P. Ring and P. Schuck, *Phys. Rev. C* **84**, 054309 (2011).
- [38] M. B. Tsang et al., *Phys. Rev. C* **86**, 15803 (2012).
- [39] B. K. Agrawal, S. K. Dhiman and R. Kumar, *Phys. Rev. C* **73**, 034319 (2006).
- [40] B. A. Brown, G. Shen, G. C. Hillhouse, J. Meng and A. Trzcińska, *Phys. Rev. C* **76**, 034305 (2007).
- [41] C. Xu, B. -A. Li and L. -W. Chen, *Phys. Rev. C* **82**, 054607 (2010).
- [42] W. G. Newton, M. Gearheart and B. -A. Li, *arXiv:1110.4043* (2011).
- [43] A. W. Steiner and S. Gandolfi, *Phys. Rev. Lett.* **108**, 081102 (2012).
- [44] F. J. Fattoyev, W. G. Newton, J. Xu and B. -A. Li, *Phys. Rev. C* **86**, 025804 (2012).
- [45] A. Klimkiewicz et al., *Phys. Rev. C* **76**, 051603 (2007).
- [46] A. Carbone, G. Colò, A. Bracco, L. -G. Cao, P. F. Bortignon, F. Camera and O. Wieland, *Phys. Rev. C* **81**, 041301 (2010).
- [47] P. Danielewicz and J. Lee, *arXiv:1111.0326v1*.
- [48] P. Möller, W. D. Meyers, H. Sagawa and S. Yoshida, *Phys. Rev. Lett.* **108**, 052501 (2012).
- [49] J. R. Oppenheimer and G. M. Volkoff, *Phys. Rev* **55**, 374 (1939); R. C. Tolman, *Phys. Rev* **55**, 364 (1939).